Band Limited Impulse Invariance Method

Nara Hahn
Institute of Sound and Vibration Research
University of Southampton, UK
nara.hahn@soton.ac.uk

Frank Schultz and Sascha Spors
Institute of Communications Engineering
University of Rostock, Germany
{frank.schultz, sascha.spors}@uni-rostock.de

***Abstract*—We propose the band-limited impulse invariance method, which models a continuous-time LTI system in the discrete-time domain with high accuracy. A given system function in the Laplace domain is realized in the z-domain as a parallel connection of IIR and FIR filters. The IIR part is obtained by using the conventional impulse invariance method, whereas the FIR part is designed in such a way that it suppresses the aliasing occurring in the IIR filter. The FIR coefficients are derived analytically from a band-limited representation of the continuous-time impulse response. The accuracy of the discrete-time model is readily adjusted by the FIR length.**

I. Introduction

Digital modeling of continuous-time systems is a common problem in signal processing. Analog devices such as audio effects and musical instruments are often emulated by digital filters [1–3]. Physical systems described by differential equations (e.g. waves) are also frequently simulated in the discrete-time domain [4–7]. Spatial signal processing techniques such as sound field analysis and synthesis often rely on analytical models describing the sound field of interest [8–12]. For linear time-invariant (LTI) systems, the transfer function in the Laplace (s) domain is converted into the z-domain and then realized as a digital filter. Well known methods for s-to-z conversion are the bilinear transform, the impulse invariance method, and the matched z-transform [13]. The resulting discrete-time systems typically exhibit spectral deviations due to aliasing and/or frequency warping. This can be mitigated by increasing the sampling frequency which comes at the expense of computational complexity and latency that might be unaffordable or intolerable in practice. One can of course resort to numerical filter design methods [14–16]. The design accuracy is, however, sensitive to the choice of the filter structure and the control frequencies. Moreover, the filter coefficients cannot be parameterized in terms of physical variables that describe the system. This might be a significant disadvantage for latency-sensitive applications.

Several approaches have been proposed to improve the accuracy of the discrete-time model. Different modifications were applied to the existing s-to-z conversion methods in order to meet certain design specifications [17–21]. Higher-order s-to-z conversion methods were presented in [22–24], mainly focusing on integrator and differentiator design. In audio applications, moderate computational cost is often traded for improved spectral accuracy which is crucial for perceived audio quality. For instance, the aliasing distortion occurring in the matched z-transform is compensated by cascading correction filters [25, 26]. In [27], Särkkä introduced a state-space model, where the differential equation describing the analog filter is numerically solved. This approach achieves high accuracy which depends on the employed interpolation order. However, calculating the coefficients is computationally demanding as it requires numerical integration and the evaluation of matrix exponential.

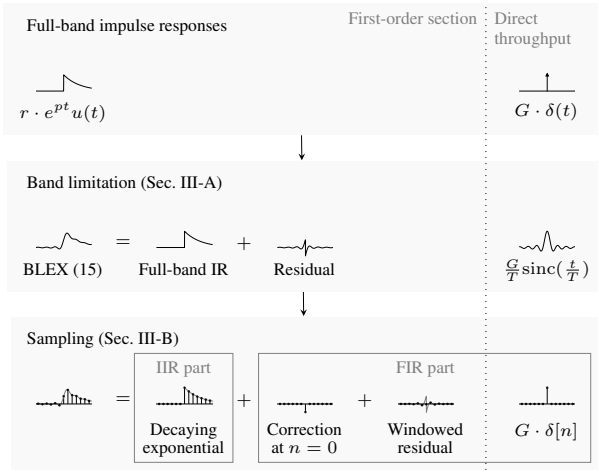

Fig. 1: The proposed band-limited impulse invariance method, applied to a single first-order section and a direct throughput (p: pole, r: residue, G: direct gain, T: sampling interval). Please refer to the respective sections for more detail.

In this paper, an improved impulse invariance method is proposed, which is inspired by the approaches for aliasing reduction in digitally emulated analog waveforms [28]. It is suited for an accurate and efficient discrete-time modeling of continuous-time systems. As depicted in Fig. 1, the presented method exploits the band-limited representations of the continuous-time impulse responses (Sec. III-A), which is realized as a parallel connection of infinite impulse response (IIR) and finite impulse response (FIR) filters. The IIR part is obtained by using the conventional impulse invariance method (Sec. II), whereas the FIR filter is designed in such a way that it cancels the aliasing occurring in the IIR filter (Sec. III-B). The design accuracy of the overall filter is controlled straightforwardly by the FIR length, as will be demonstrated by numerical simulations (Sec. III-C).

II. Impulse Invariance Method

This section briefly reviews the impulse invariance method with the focus on different correction schemes. Let us consider a continuous-time system represented by a partial fraction expansion in the Laplace domain ($s = \sigma + i\omega$ where $\sigma, \omega \in \mathbb{R}$),

$$H_\mathrm{a}(s) = \frac{B(s)}{A(s)} = G + \sum_{k=0}^{K-1} \frac{r_k}{s - p_k}, \tag{1}$$

where $p_k \in \mathbb{C}$ denote simple poles and $r_k \in \mathbb{C}$ the corresponding residues. The direct throughput has a frequency-independent gain $G \in \mathbb{R}$. The system function is proper, meaning that the numerator $B(s)$ and denominator $A(s)$ are of the same order K. The system is assumed to be causal and stable. The inverse Laplace transform of (1) yields the continuous-time impulse response [29, Ch. 4],

$$h_\mathrm{a}(t) = G \cdot \delta(t) + \sum_{k=0}^{K-1} r_k \, e^{p_k t} \, u(t), \tag{2}$$

where $\delta(t)$ denotes the Dirac delta function and $u(t)$ the Heaviside step function [30, Eq. (1.16)]. Without loss of generality, only a single first-order section ($K = 1$) will be considered in the following. The subscript k is thus dropped.

In the impulse invariance method, a continuous-time system is realized as a digital filter whose impulse response $h[n]$ is derived by an ideal time-domain sampling of the continuous-time impulse response $h_\mathrm{a}(t)$ [31, Sec. 7.3],

$$h[n] = T \cdot h_\mathrm{a}(nT), \quad n \in \mathbb{Z}, \tag{3}$$

with T denoting the sampling period. However, the sampling of $h_\mathrm{a}(t)$ is not trivial due to the peculiarities of $\delta(t)$ and $u(t)$ at $t = 0$.

Strictly speaking, the impulse invariance method cannot be applied to the direct throughput $G \cdot \delta(t)$. Since the Dirac delta function has an infinite bandwidth, sampling the impulse response yields aliasing with unbounded energy. Nevertheless, the frequency-independent gain can be readily realized in the discrete-time as a weighted unit impulse $\delta[n]$,

$$G \cdot \delta[n], \tag{4}$$

whose z-transform is G. As will be shown in Sec. III, this constitutes an ideal band-limitation followed by sampling.

The impulse response of a single one-pole system, described by the right-sided exponential function in (2), is commonly discretized in the form of

$$h[n] = rT \cdot e^{pTn}\big(u[n] + d \cdot \delta[n]\big), \tag{5}$$

where $u[n]$ denotes the discrete-time unit step function,

$$u[n] = \begin{cases} 0, & n < 0 \\ 1, & n \geq 0. \end{cases} \tag{6}$$

Note that the sampled value at the jump discontinuity ($t = 0$) depends on the correction term d. The z-transform of (5) reads

$$H^{(\mathrm{IIM})}(z) = \frac{rT}{1 - e^{pT} z^{-1}} + rdT, \tag{7}$$

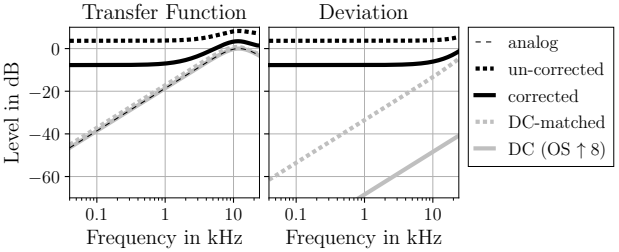

Fig. 2: Digital modeling of a second-order band-pass filter ($f_\mathrm{c} = 12\,\mathrm{kHz}$, $Q = \frac{1}{\sqrt{2}}$, $f_\mathrm{s} = 48\,\mathrm{kHz}$) using the impulse invariance method with varying correction term d. Left: spectrum of the digital filters. Right: deviation from the analog spectrum.

which consists of a one-pole IIR filter and a constant. Equation (7) can be alternatively expressed as

$$H^{(\mathrm{IIM})}(z) = rT(1 + d)\frac{1 - \frac{d}{1+d} e^{pT} z^{-1}}{1 - e^{pT} z^{-1}}, \tag{8}$$

where a zero appears at $z = \frac{d}{1+d} e^{pT}$.

The impulse invariance method is commonly introduced with $d = 0$ which leads to

$$H^{(\mathrm{IIM})}(z) = \frac{rT}{1 - e^{pT} z^{-1}}. \tag{9}$$

It was pointed out in [31, Sec. 7.3] that evaluating (9) for $z = e^{i\omega T}$ deviates from the periodic repetition of the continuous-time spectrum,

$$\sum_{\mu \in \mathbb{Z}} H_\mathrm{a}\left(i(\omega - \mu \cdot \omega_\mathrm{s})\right) = \sum_{\mu \in \mathbb{Z}} \frac{r}{i(\omega - \mu \cdot \omega_\mathrm{s}) - p}, \tag{10}$$

where $\omega_\mathrm{s} = 2\pi f_\mathrm{s} = \frac{2\pi}{T}$ denotes the angular sampling frequency. In the so-called *corrected* impulse invariance method [31–33], this deviation was accounted for and the sampled value of $u(t)$ at $t = 0$ was set to $\frac{1}{2}\left[u(0_-) + u(0_+)\right] = \frac{1}{2}$ [34, Ch. 5]. The corresponding correction term is thus $d = -\frac{1}{2}$, yielding

$$H^{(\mathrm{CIIM})}(z) = \frac{rT}{2}\frac{1 + e^{pT} z^{-1}}{1 - e^{pT} z^{-1}}. \tag{11}$$

It is important to note that the above-mentioned correction only assures that (9) equals the aliased spectrum (10). In this regard, the corrected impulse invariance method might not be suitable if an accurate modeling of the analog filter is of primary interest. The accuracy of the filter can be improved by matching the spectrum (7) to its continuous-time counterpart $\frac{r}{i\omega - p}$ at a reference frequency ω_ref [35, Sec. 6.3],

$$\frac{r}{i\omega_\mathrm{ref} - p} = rT\left(\frac{1}{1 - e^{(p - i\omega_\mathrm{ref})T}} + d\right). \tag{12}$$

Solving this with respect to d yields

$$d = \frac{1}{T(i\omega_\mathrm{ref} - p)} - \frac{1}{1 - e^{(p - i\omega_\mathrm{ref})T}}. \tag{13}$$

Matching the frequency response at DC ($\omega_{\mathrm{ref}} = 0$) generally leads to an improved result throughout a wide frequency range [17, 18].

In order to examine the influence of the correction term d, a second-order band-pass filter is considered [36, Eq. (5.25)],

$$H_{\mathrm{a}}(s) = \frac{\frac{1}{Q}\left(\frac{s}{\omega_{\mathrm{c}}}\right)}{\left(\frac{s}{\omega_{\mathrm{c}}}\right)^2 + \frac{1}{Q}\left(\frac{s}{\omega_{\mathrm{c}}}\right) + 1}. \tag{14}$$

The center frequency is set to $\omega_{\mathrm{c}} = 2\pi f_{\mathrm{c}}$ with $f_{\mathrm{c}} = 12\,\mathrm{kHz}$ and the quality factor to $Q = \frac{1}{\sqrt{2}}$. The sampling frequency is $f_{\mathrm{s}} = 48\,\mathrm{kHz}$. As depicted in Fig. 2 (indicated by ---), this is a critical example since the peak is just one octave below the Nyquist frequency $\frac{f_{\mathrm{s}}}{2} = 24\,\mathrm{kHz}$ and the high-frequency spectrum decays slowly at a rate of $-20\,\mathrm{dB/decade}$. The magnitude responses of the digital filters $|H(e^{i\omega T})|$ are shown on the left and the spectral deviations $|H(e^{i\omega T}) - H_{\mathrm{a}}(i\omega)|$ on the right. The un-corrected (⋯) as well as the corrected (—) impulse invariance methods exhibit strong deviations, failing to model the analog filter. The benefit of the DC-matching scheme (⋯) is apparent. Further improvement is achieved by increasing the sampling rate (—), where the computational cost scales with the oversampling factor.

III. Band Limited Impulse Invariance Method

The aliasing occurring in the impulse invariance method is attributed to the infinite bandwidth of the prototype analog filter. In this section, the IIR filter obtained from the conventional method is combined in parallel with an FIR filter (see Fig. 1) in order to cancel the aliasing. The presented method is in the same spirit as the approaches introduced in [28].

A. Band Limited Impulse Responses

For an aliasing-free sampling, the bandwidth has to be limited to $|\omega| < \frac{\omega_{\mathrm{s}}}{2}$. An ideally band-limited impulse response of a one-pole system $\frac{r}{s-p}$ is obtained by the inverse Laplace transform along the imaginary axis ($s = 0 + i\omega$) [35, Sec. 6.3],

$$\underbrace{h_{\mathrm{a}}^{(\mathrm{BL})}(t)}_{\text{BLEX}} = \frac{r}{2\pi i}\int_{-i\frac{\omega_{\mathrm{s}}}{2}}^{+i\frac{\omega_{\mathrm{s}}}{2}} \frac{e^{st}}{s-p}\,\mathrm{d}s = \underbrace{r\cdot e^{pt}u(t)}_{\text{Full-band IR}} + \underbrace{r\cdot\varepsilon(t)}_{\substack{\text{BLEX}\\ \text{residual}}}, \tag{15}$$

where

$$\varepsilon(t) = \begin{cases} \frac{e^{pt}}{2\pi i}\left[E_1\left((i\frac{\omega_{\mathrm{s}}}{2}+p)t\right) - E_1\left((-i\frac{\omega_{\mathrm{s}}}{2}+p)t\right)\right], & t \neq 0 \\ \frac{1}{2\pi i}\left[\ln(i\frac{\omega_{\mathrm{s}}}{2}-p) - \ln(-i\frac{\omega_{\mathrm{s}}}{2}-p)\right] - u(0), & t = 0. \end{cases} \tag{16}$$

with $E_1(\cdot) \coloneqq \int_z^\infty \frac{e^{-z'}}{z'}\mathrm{d}z'$ denoting the exponential integral function [37, Eq. (5.1.1)]. Equation (15) is derived by exploiting the contour integral $\frac{r}{2\pi i}\oint_C \frac{e^{st}}{s-p}\mathrm{d}s$ in the complex plane. As illustrated in Fig. 3, the contour C is drawn in the right half-plane for $t < 0$ and in the left half-plane for $t > 0$. Due to the singularity at $s = p$, the exponential term $r \cdot e^{pt}$ appears for $t > 0$, which follows from the residue theorem [38, Ch. 4]. The value at $t = 0$ is obtained by the indefinite integral $\ln(z) = \int \frac{1}{z'}\mathrm{d}z'$ [30, Eq. (4.10.1)], where the principal value (i.e. $\Im\{\ln(z)\} \in (-\pi, \pi]$) is chosen. In the remainder, $h_{\mathrm{a}}^{(\mathrm{BL})}(t)$ will be referred to as the band-limited exponential (BLEX) function and $r \cdot \varepsilon(t)$ as the BLEX residual.

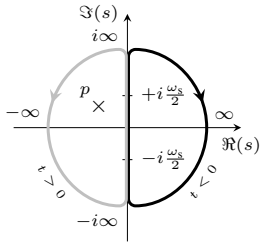

Fig. 3: Integral path of $\frac{r}{2\pi i}\oint_C \frac{e^{st}}{s-p}\mathrm{d}s$ on the complex plane for $t < 0$ (—) and $t > 0$ (—). The location of the pole p is indicated by $\times$. The system is assumed to be stable and thus $\Re(p) < 0$.

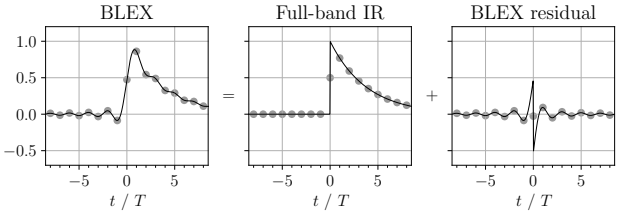

Fig. 4: Impulse response of a one-pole system ($p = -2\pi \cdot 1000\,\mathrm{rad/s}$, $r = 1$). Left: BLEX function (15), Center: Full-band impulse response, Right: BLEX residual. The filled circles (●) indicate the sampled values for $f_{\mathrm{s}} = 48\,\mathrm{kHz}$. The amplitude scaling T is omitted for the ease of visualization.

The band-limited impulse invariance method proposed in this paper is based on (15), which states that an ideal band limitation can be applied to a prototype filter by superposing the corresponding BLEX residual onto the full-band impulse response. This implies that the BLEX residual exhibits an ideally high-pass filtered spectrum which cancels the components outside the base band ($|\omega| > \frac{\omega_{\mathrm{s}}}{2}$). Fig. 4 shows an exemplary BLEX function along with the full-band impulse response and the corresponding BLEX residual.

The band-limited impulse response of the direct part can be derived in a similar fashion by the inverse Fourier transform,

$$\frac{1}{2\pi}\int_{-\frac{\omega_{\mathrm{s}}}{2}}^{+\frac{\omega_{\mathrm{s}}}{2}} G\cdot e^{i\omega t}\,\mathrm{d}\omega = \frac{G\sin(\frac{\omega_{\mathrm{s}}}{2}t)}{\pi t} = \frac{G}{T}\cdot\mathrm{sinc}(f_{\mathrm{s}}t), \tag{17}$$

where $\mathrm{sinc}(x) \coloneqq \frac{\sin(\pi x)}{\pi x}$ denotes the sinc function.

B. Filter Design

The impulse invariance method (3) is now applied to the band-limited representations derived in III-A. The decaying exponential will be realized as an IIR filter whereas the BLEX residual and the direct throughput as an FIR filter (Fig. 1).

Note from Fig. 4 (right) that the BLEX residual function is noncausal and has an infinite temporal extent. For practical usage, it needs to be truncated to a finite length and tapered by a window function. This inevitably results in a nonideal

high-pass characteristic of the BLEX residual. The length of the sampled BLEX residual is denoted by $L = M + N$ where M and N respectively correspond to the noncausal ($n < 0$) and causal ($n \geq 0$) parts. In order to build a causal filter, a pre-delay of $\tau = M \cdot T$ is introduced to the prototype system, modifying the target transfer function to $H_\mathrm{a}(i\omega)\, e^{-i\omega\tau}$.

The sampling of the BLEX residual reads (cf. (3) and (16))

$$h^{(\mathrm{res})}[n] = rT\, \varepsilon\big((n-M)T\big) \cdot v[n], \tag{18}$$

for $n = 0, \ldots, L-1$, where $v[n]$ denotes a window function of the same length. The exponential integral function $E_1(\cdot)$ in (16) can be evaluated efficiently by using a power series or continued fraction [39, 40]. It is implemented by `scipy.special.exp1` in Python and by `expint` in Matlab. The impulse response of the delayed IIR filter is (cf. (5))

$$h^{(\mathrm{pole})}[n] = rT\, e^{pT(n-M)} \Big(u[n-M] + d \cdot \delta[n-M] \Big). \tag{19}$$

Similar to the conventional impulse invariant method (Sec. II), the offset of the spectrum at a reference frequency can be corrected by adjusting d. The DC-matching scheme, for instance, yields

$$d = -\frac{1}{pT} - \frac{1}{1-e^{pT}} - \sum_{n=0}^{L-1} \varepsilon((n-M)T) \cdot v[n], \tag{20}$$

where the sum corresponds to the DC response (z-transform with $z = e^{i0} = 1$) of the windowed BLEX residual. The direct throughput is realized as an integer delay with gain G,

$$h^{(\mathrm{dir})}[n] = T \cdot \frac{G}{T} \operatorname{sinc}\left(f_\mathrm{s} T \cdot (n-M)\right) = G \cdot \delta[n-M], \tag{21}$$

which follows from (3) and (17). The z-domain expressions of (18), (19), and (21) read

$$H^{(\mathrm{res})}(z) = \sum_{n=0}^{L-1} h^{(\mathrm{res})}[n]\, z^{-n} \tag{22}$$

$$H^{(\mathrm{pole})}(z) = z^{-M} \Big(\frac{rT}{1-e^{pT} z^{-1}} + rdT \Big) \tag{23}$$

$$H^{(\mathrm{dir})}(z) = G \cdot z^{-M}, \tag{24}$$

respectively. The recursive part $\frac{rT}{1-e^{pT}z^{-1}}$ of $H^{(\mathrm{pole})}(z)$ is realized as an IIR filter, which corresponds to the un-corrected impulse invariance method (9). Note that (23) and (24) both include a delay of M samples. The nonrecursive parts are combined and realized as an FIR filter of length L,

$$H^{(\mathrm{FIR})}(z) = z^{-M} \cdot \big(G + rdT\big) + \sum_{n=0}^{L-1} h^{(\mathrm{res})}[n] z^{-n}, \tag{25}$$

i.e. the windowed BLEX residual $H^{(\mathrm{res})}(z)$, the correction term $rdT \cdot z^{-M}$ in $H^{(\mathrm{pole})}(z)$, and the direct throughput $H^{(\mathrm{dir})}(z)$.

The presented approach can be readily extended to higher-order filters ($K > 1$) described by the partial fraction expansion (1),

$$H(z) = \underbrace{z^{-M} \Big(G + \sum_{k=0}^{K-1} r_k d_k T \Big) + \sum_{k=0}^{K-1} H_k^{(\mathrm{res})}(z)}_{H^{(\mathrm{FIR})}(z)} + z^{-M} \sum_{k=0}^{K-1} \underbrace{\frac{r_k T}{1 - e^{p_k T} z^{-1}}}_{H_k^{(\mathrm{IIR})}(z)}, \tag{26}$$

where the subscript k is re-introduced. Note that the correction terms, the direct throughput, and the individual BLEX residual functions are implemented as a single FIR filter $H^{(\mathrm{FIR})}(z)$. The overall system is a parallel connection of an FIR filter and equally delayed IIR filters. If necessary, IIR filters with complex conjugate poles can be combined into second-order section filters (biquads).

The filter described by (26) bears some similarity to the state-space model introduced in [27]. If formulated as a rational transfer function, the accuracy of both methods depends on the numerator order. Also, a pre-delay is introduced to the filters which is associated with the band limitation. The computational cost of the state-space model and the proposed method respectively depend on the numerical integration scheme and the evaluation of $E_1(\cdot)$. A rigorous comparison remains beyond the scope of this paper.

It is worth noting that $h^{(\mathrm{res})}[n]$ and $h^{(\mathrm{pole})}[n]$ overlap for $n = M+1, \ldots, L$. If the aliasing is of considerable amount, those impulse responses will have large amplitudes with opposing polarity in this interval, canceling most of the energy from each other. As Bank and Smith pointed out in [15], such a filter might have scaling issues in fixed-point processing. A higher dynamic range can be maintained by moving the early part of the IIR part to the FIR filter and applying a delay and attenuation to the IIR filter [41]. The resulting filter will then have the same structure as the delayed parallel filters introduced in [15]. This modification is not considered in the following evaluation (Sec. III-C) which is performed in double precision.

C. Evaluation

The proposed method is applied to the same second-order filter (14) considered in Fig. 2. The FIR coefficients are computed according to (26), where the BLEX residuals are windowed with a Kaiser window ($\beta = 8.6$). The FIR length is set to odd numbers $L = 5, 11, 21, 41$. The beginning of the IIR filters is aligned with the center of the FIR filter (i.e. $M = \frac{L-1}{2}$). The spectral deviations are evaluated as $|H(e^{i\omega T}) - H_\mathrm{a}(i\omega) e^{-i\omega\tau}|$ by taking the pre-delay into account. As depicted in Fig. 5, increasing L systematically improves the performance of the digital filter. The magnitude spectrum of the FIR part ($L = 41$) shown in Fig. 5 ($\cdots$) is in a close agreement with the deviation of the un-corrected impulse invariance method depicted in Fig. 2 (right). This shows that

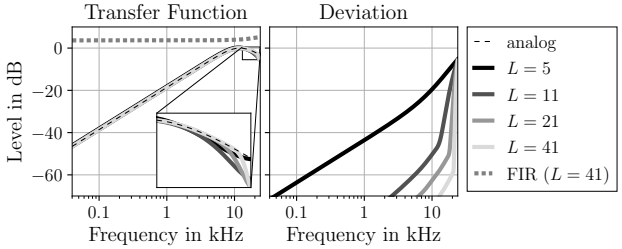

Fig. 5: Digital modeling of a second-order band-pass filter ($f_\mathrm{c} = 12\,\mathrm{kHz}$, $Q = \frac{1}{\sqrt{2}}$, $f_\mathrm{s} = 48\,\mathrm{kHz}$) using the proposed method. Left: spectrum of the digital filters. Right: deviation from the analog spectrum.

the aliasing occurring in the conventional method is canceled by the BLEX residual functions. Up to $10\,\mathrm{kHz}$, the proposed method with $L = 11$ is comparable to the conventional impulse invariant method with an oversampling by a factor of 8 (cf. Fig. 2).

IV. Conclusion

An accurate yet efficient method is presented for the discrete-time modeling of continuous-time LTI systems. The resulting filter has an interpretable structure where the aliasing occurring in the IIR filters is explicitly reduced by using the FIR filter. The proposed method can be used not only for traditional filter design but also for the simulation of physical systems (e.g. mechanical, electrical, and acoustical) that are described by rational system functions. The implementations generating Fig. 2, Fig. 4 and Fig. 5 are available [42].

References

[1] U. Zölzer, X. Amatriain, D. Arfib, J. Bonada, G. De Poli, P. Dutilleux *et al.*, *DAFX - Digital Audio Effects*. Chichester, UK: Wiley, 2002.

[2] J. O. Smith, *Physical Audio Signal Processing*. http://ccrma.stanford.edu/~jos/pasp/, 2010, accessed 23 July. 2021.

[3] V. Välimäki and J. D. Reiss, "All about audio equalization: Solutions and frontiers," *Appl. Sci.*, vol. 6, no. 5, pp. 1–46, 2016.

[4] K. Yee, "Numerical solution of initial boundary value problems involving Maxwell's equations in isotropic media," *IEEE Trans. Antennas Propag.*, vol. 14, no. 3, pp. 302–307, 1966.

[5] S. Bilbao, *Numerical Sound Synthesis: Finite Difference Schemes and Simulation in Musical Acoustics*. Chichester, UK: Wiley, 2009.

[6] L. Greengard, T. Hagstrom, and S. Jiang, "The solution of the scalar wave equation in the exterior of a sphere," *J. Comput. Phys.*, vol. 274, pp. 191–207, 2014.

[7] P. Martin, "Acoustic scattering by a sphere in the time domain," *Wave Motion*, vol. 67, pp. 68–80, 2016.

[8] N. A. Gumerov and R. Duraiswami, *Fast Multipole Methods for the Helmholtz Equation in Three Dimensions*. Oxford, UK: Elsevier, 2005.

[9] A. Kuntz, *Wave Field Analysis Using Virtual Circular Microphone Arrays*. Munich, Germany: Verlag Dr. Hut, 2009.

[10] J. Ahrens, *Analytic Methods of Sound Field Synthesis*. Berlin, Germany: Springer, 2012.

[11] B. Rafaely, *Fundamentals of Spherical Array Processing*. Berlin, Germany: Springer, 2015.

[12] F. Zotter and M. Frank, *Ambisonics*. Springer, 2019.

[13] J. G. Proakis and D. G. Manolakis, *Digital Signal Processing: Principles, Algorithms, and Applications*. Upper Saddle River, NJ, USA: Prentice-Hall, 1996.

[14] T. W. Parks and C. S. Burrus, *Digital Filter Design*. Chichester, UK: Wiley, 1987.

[15] B. Bank and J. O. Smith III, "A delayed parallel filter structure with an FIR part having improved numerical properties," in *Proc. of Audio Eng. Soc. (AES) Conv.*, Berlin, Germany, Apr. 2014.

[16] T. Schmidt and J. Bitzer, "Digital equalization filter: New solution to the frequency response near Nyquist and evaluation by listening tests," in *Proc. 128th Audio Eng. Soc. (AES) Conv.*, London, UK, May 2010.

[17] D. B. Miron, "On corrections to a z-transform method for FDTD simulations with frequency-dependent dielectric functions," *IEEE Trans. Antennas Propag.*, vol. 58, no. 12, pp. 4100–4104, 2010.

[18] Z. Lin and L. Thylen, "On the accuracy and stability of several widely used FDTD approaches for modeling Lorentz dielectrics," *IEEE Trans. Antennas Propag.*, vol. 57, no. 10, pp. 3378–3381, 2009.

[19] M. Massberg, "Digital low-pass filter design with analog-matched magnitude response," in *Proc. 131st Audio Eng. Soc. (ASE) Conv.*, New York, NY, USA, Oct. 2011.

[20] D. P. Berners and J. S. Abel, "Discrete-time shelf filter design for analog modeling," in *Proc. 115th Audio Eng. Soc. (AES) Conv.*, New York, NY, USA, Oct. 2003.

[21] S. J. Orfanidis, "Digital parametric equalizer design with prescribed Nyquist-frequency gain," *J. Audio Eng. Soc.*, vol. 45, no. 6, pp. 444–455, 1997.

[22] M. A. Al-Alaoui, "Novel stable higher order s-to-z transforms," *IEEE Trans. Circuits Syst. I*, vol. 48, no. 11, pp. 1326–1329, 2001.

[23] ——, "Novel approach to anaog-to-digital transforms," *IEEE Trans. Circuits Syst. I*, vol. 54, no. 2, pp. 338–350, 2007.

[24] S. C. Pei and H. J. Hsu, "Fractional bilinear transform for analog-to-digital conversion," *IEEE Trans. Signal Process.*, vol. 56, no. 5, pp. 2122–2127, 2008.

[25] J. Flynn and J. D. Reiss, "Improving the frequency response magnitude and phase of analogue-matched digital filters," in *Proc. 144th Audio Eng. Soc. (AES) Conv.*, Milan, Italy, May 2018.

[26] D. W. Gunness and O. S. Chauhan, "Optimizing the magnitude response of matched z-transform filters ("MZTI") for loudspeaker equalization," in *Proc. 32nd Audio Eng. Soc. (AES) Int. Conf.*, Hillerød, Denmark, 2007.

[27] S. Särkkä and A. Huovilainen, "Accurate discretization of analog audio filters with application to parametric equalizer design," *IEEE Trans. Audio Speech Lang. Process.*, vol. 19, no. 8, pp. 2486–2493, 2011.

[28] V. Välimäki and A. Huovilainen, "Antialiasing oscillators in subtractive synthesis," *IEEE Signal Process. Mag.*, vol. 24, no. 2, pp. 116–125, 2007.

[29] B. Girod, R. Rabenstein, and A. Stenger, *Signals and Systems*. Chichester, UK: Wiley, 2001.

[30] F. W. J. Olver, D. W. Lozier, R. F. Boisvert, and C. W. Clark, *NIST Handbook of Mathematical Functions Handback*. New York, NY, USA: Cambridge Univ. Press, 2010.

[31] R. A. Gabel and R. A. Roberts, *Signals and Linear Systems*. New York, NY, USA: Wiley, 1973.

[32] W. F. Mecklenbräuker, "Remarks on and correction to the impulse invariant method for the design of IIR digital filters," *Signal Process.*, vol. 80, no. 8, pp. 1687–1690, 2000.

[33] L. B. Jackson, "A correction to impulse invariance," *IEEE Signal Process. Lett.*, vol. 7, no. 10, pp. 273–275, 2000.

[34] R. N. Bracewell, *The Fourier Transform and its Applications*. New York, NY, USA: McGraw-Hill, 1986.

[35] D. Schlichthärle, *Digital filters*. Berlin, Germany: Springer, 2014.

[36] U. Zölzer, *Digital Audio Signal Processing*. Chichester, UK: Wiley, 2008.

[37] M. Abramowitz and I. A. Stegun, *Handbook of Mathematical Functions: with Formulas, Graphs, and Mathematical Tables*. New York, NY, USA: Dover, 1964.

[38] M. J. Ablowitz and A. S. Fokas, *Complex Variables: Introduction and Applications*. New York, NY, USA: Cambridge Univ. Press, 2003.

[39] W. J. Cody, "Algorithm 715: SPECFUN–a portable FORTRAN package of special function routines and test drivers," *ACM Trans. Math. Software*, vol. 19, no. 1, pp. 22–30, 1993.

[40] D. M. Smith, "Algorithm 911: Multiple-precision exponential integral and related functions," *ACM Trans. Math. Software*, vol. 37, no. 4, pp. 1–16, 2011.

[41] B. Bank, "Converting infinite impulse response filters to parallel form," *IEEE Signal Process. Mag.*, vol. 35, no. 3, pp. 124–130, 2018.

[42] N. Hahn, "Band limited impulse invariant method," Feb. 2022. [Online]. Available: https://github.com/spatialaudio/band-limited-impulse-invariance-method